An Electrostatically Embedded QM/MM Scheme for Electrified Interfaces

Nawras Abidi, Stephan N. Steinmann

An Electrostatically Embedded QM/MM Scheme for Electrified Interfaces

Nawras Abidi and Stephan N. Steinmann*

Ecole Normale Supérieure de Lyon, CNRS, Laboratoire de Chimie UMR 5182, 46 allée d'Italie, F-69364, LYON, France

E-mail: stephan.steinmann@ens-lyon.fr

Phone: (+33)4 72 72 81 55

Abstract

Atomistic modelling of electrified interfaces remains a major issue for detailed insights in electrocatalysis, corrosion, electrodeposition, batteries and related devices such as pseudocapacitors. In these domains, the use of grand-canonical density functional theory (GC-DFT) in combination with implicit solvation models has become popular. GC-DFT can be conveniently applied not only to metallic surfaces, but also to semi-conducting oxides and sulfides and is, furthermore, sufficiently robust to achieve a consistent description of reaction pathways. However, the accuracy of implicit solvation models for solvation effects at interfaces is in general unknown. One promising way to overcome the limitations of implicit solvents is going towards hybrid quantum mechanical (QM)/molecular mechanics (MM) models. For capturing the electrochemical potential dependence, the key quantity is the capacitance, i.e., the relation between the surface charge and the electrochemical potential. In order to retrieve the electrochemical potential from a QM/MM hybrid scheme, an electrostatic embedding is required. Furthermore, the charge of the surface and of the solvent regions have to be strictly opposite in order to consistently simulate charge-neutral unit cells in MM

and in QM. To achieve such a QM/MM scheme, we present the implementation of electrostatic embedding in the popular VASP code. This scheme is broadly applicable to any neutral or charged solid/liquid interface. Here, we demonstrate its use in the context of GC-DFT for the hydrogen evolution reaction (HER) over a noble-metal-free electrocatalyst, MoS_2. We investigate the effect of electrostatic embedding compared to the implicit solvent model for three contrasting active sites on MoS_2: (i) the sulfur vacancy defect which is rather apolar. (ii) an Mo anti-site defect, where the active site is a surface bound highly polar OH group and (iii) a reconstructed edge site which is generally believed to be responsible for most of the catalytic activity. According to our results, the electrostatic embedding leads to almost indistinguishable results compared to the implicit solvent for the apolar system, but has a significant effect on polar sites. This demonstrates the reliability of the hybrid QM/MM, electrostatically embedded solvation model for electrified interfaces.

Keywords

grand-canonical DFT, hydrogen evolution reaction, electrified interfaces, QM/MM, solvation

1 Introduction

Modelling electrified interfaces is one of the central aspects to reach a detailed understanding of energy storage (batteries, pseudo-/super-capacitors) and conversion (electrolysers and fuel cells) devices, but also for corrosion and metal-deposition.[1] In the presence of a liquid electrolyte a "double layer" forms at these electrified interfaces: The surface charge is compensated by a charge distribution of the electrolyte in solution. The models for the electrochemical double layer have a long history and continue to be refined,[2,3] given that experimentally probing the nature of the double layer remains very challenging.[4]

From an atomistic modelling point of view, the ideal would be to model the entire system

with explicit atoms and electrons, such that the most realistic and accurate description is reached. However, this is first limited by the available computing power (solid/liquid interfaces need $\sim$ 500 ps equilibration times for thousands of atoms) and second accounting for the electrochemical potential is not trivial, as the surface charge needs to be modulated and the effective potential measured.[5–7]

The development of grand-canonical DFT (GC-DFT) in its most general formulation goes back to Mermin[8] and was reformulated as a Legendre transform by Nalewajski and Parr.[9] Some 30 years after its first formulation, GC-DFT has been recognized as useful for applications to electrified interfaces,[10] and it is only the last 10-15 years that GC-DFT has become popular for modelling electrocatalysis[11–13] and elementary reaction steps in batteries.[14] While a detailed derivation of GC-DFT can be found in the literature,[9,15–17] we here just give the main working equation and how it is evaluated in practice. At an electrified interface, the relevant thermodynamic ensemble is grand-canonical: Since the system is in contact with a reservoir of electrons at potential μ, the number of electrons (N) fluctuates. Hence, one needs to consider the grand-potential Ω:

$$\Omega(\nu, \mu) = E(\nu, \mu) - \mu \cdot N \tag{1}$$

where ν is the external potential, i.e., due to the nuclear charges and $E(\nu, \mu)$ is the corresponding canonical energy.

In practice, electronic structure codes work rather with the system charge $q = N - N_0$, where N_0 corresponds to the neutral system with the external potential ν and thus provide the electronic energy $E(q)$ and the corresponding work function ($\mu(q)$) as a function of the charge. Note, that for a conducting system the electronic energy $E(q)$ is a linear function of the charge, and can be exploited to retrieve the corresponding work function.[9,18] Furthermore, one can convert the "absolute" electron potential (i.e., with respect to the energy of an electron in vacuum) μ, to the more conventional electrochemical potential vs

SHE, i.e., $U = \mu(q)$-4.44 eV. For convenience, Eq. 1 is sometimes restated as:

$$G(U) \approx E(q) - \mu(q) \cdot q \tag{2}$$

which highlights "practical" aspects of obtaining electrochemical potential dependent (free) energies: Standard computations of Gibbs free energies as a function of the charge and measuring the corresponding workfunctions. If thermal corrections are included, the approximate sign becomes an equal sign.

Applications of GC-DFT to liquid-phase electrocatalysis heavily rely on approximate methods to describe (a) the charge of the double layer (that has to neutralize the periodic unit cells in order to achieve finite Coulomb potentials) and (b) the solvent. Various formulations of implicit solvents have been developed and, when formulated as including ionic species, allow to address both points together.[19] Similarly to the implicit solvents, molecular DFT,[20] joint molecular/electronic DFT[15] or the closely related reference interaction site model[21] can be exploited to provide a reasonable description of the solvent. Finally, if one accepts a uniform countercharge, the solvent can also be described explicitly at the DFT level, either via geometry optimizations[22] or molecular dynamics.[23,24]

When investigating elementary pathways of electrocatalytic reactions or solvent decompositions at the solid-electrolyte interphase of batteries,[25] the most efficient compromise between model accuracy and computational cost is reached when GC-DFT is combined with an implicit solvent and an electrolyte distribution that is described by the (modified) Poisson-Boltzmann equation.[17,26,27] Compared to simulations with explicit solvent and electrolyte molecules, the implicit solvent-electrolyte ensures a black-box, consistent treatment of the solvent-solute interactions, which is crucial for reaction pathways with intermediates of different sizes and polarities. Models that combine implicit solvent models for the bulk solvation effects with micro-solvation for more specific solvent effects have been successfully applied, but come with their own problems of achieving a consistent treatment along reaction

pathways and as a function of the electrochemical potential.[28]

Many flavors of implicit solvent/electrolyte models have been[15,26,27] and still are[19,29–32] developed and applied over the years, but they all require some fitting to experimental solvation energies. Experimental solvation energies are well established for small molecules, but only a handful of numbers are available for solid/liquid interfaces. Furthermore, implicit solvent models have intrinsic limitations for capturing near-chemisorption of the solvent at the interface, as this interaction is strongly material dependent, in contrast with the more universal electrostatic and van der Waals-type of interactions encountered for molecular solutes. Instead of system-specific tuning of parameters,[33] several research groups have pushed for hybrid solvation schemes, where the (surface) reactions are described at the density functional theory (DFT) level and the solvent effects are captured by molecular mechanics (MM).[34–36] MM is many orders of magnitudes less expensive than DFT and, therefore, extensive phase-space sampling of the liquid is easily in reach. Furthermore, compared to implicit solvents, it is clearer how to improve the quality of the description of the interface energetics: Force fields can be tested against DFT and system-specifically improved.[37,38] As an example, we have shown that a purpose-built force field for the interaction of water with the Pt(111) surface[39] leads to a semi-quantitative agreement with experiment for the adsorption of phenol and benzene on Pt(111), while the standard implicit solvent gives qualitatively wrong results when comparing the adsorption in the gas-phase with adsorption form the liquid.[40] Similarly, good agreement between DFT and MM solvation energies have been achieved at the alumina/water interface.[41] Concurrently, MM is inherently able to capture entropic solvation effects, a topic that remains challenging for implicit solvent models even for small molecules.[42]

When moving from neutral surfaces to electrified (and thus charged) surfaces one faces a conceptual issue: given that the energy of a charged periodic system is infinite, the solvation energy is no longer well defined. As a result, one cannot separately compute the energy of the system at the DFT and at the MM level to obtain a hybrid QM/MM energy. In-

stead, what is known as an "electrostatic embedding" is necessary: The DFT computations are performed in presence of a counter-charge that is derived from the MM phase-space sampling, in analogy to the coupling between molecular and electronic DFT.[20] Electrostatic embedding for determining solvation energies has been mostly explored for neutral molecular systems.[43–45] Only very recently (and independently from us), such an approach has been applied to electrified interfaces.[46,47] Even though charged interfaces are common, not only for electrified systems, but are also typical for oxide surfaces as a function of pH, electrostatic embedding is only rarely available in plane-waves codes, with the notable exceptions being GPAW,[48] Quantum Espresso[48,49] and CPMD.

Here we report the implementation of electrostatic embedding in the widely used VASP code by relying on a VASPsol[31]-based interface. The electrostatic embedding is completely general, i.e., it can handle any distribution of charges from 1 to millions and neutral or charged systems. This allows us to apply GC-DFT at an approximate QM/MM level and to demonstrate the difference between the implicit solvent and the electrostatic embedding at the particular example of the hydrogen evolution reaction (HER) over MoS_2.

2 Theoretical Background and Methods: Simplified QM/MM Solvation Energies for Charged Interfaces

An alternative to implicit solvation at the solid/liquid interface has been introduced by several groups in the form of (approximate) QM/MM schemes.[34–36] The solvation energy ΔG_{solv} as obtained by QM/MM methods is most usefully decomposed into two components:

$$\Delta G_{solv} = G_{el} + G_{non-el} \tag{3}$$

where G_{el} is the electrostatic interaction between the solvent and the solute and G_{non-el} covers the remaining, non-electrostatic, interaction free energies, i.e., the Lennard-Jones

interactions in the case of "standard" force fields, but also near-chemisorption terms as described by the GAL family of force fields.[37–39]

In the most straight forward (and most approximate) QM/MM scheme, ΔG_{solv} is determined exclusively at the MM level of theory via free energy perturbation (FEP)[50] or thermodynamic integration (TI).[40]

$$\Delta G_{solv}^{MMsolv} = G_{el}^{MM} + G_{non-el}^{MM} \tag{4}$$

This mechanical embedding approach, called MMsolv, has been shown to accurately capture the competition between adsorption of aromatic molecules and water on Pt(111) when compared to experiment.[40]

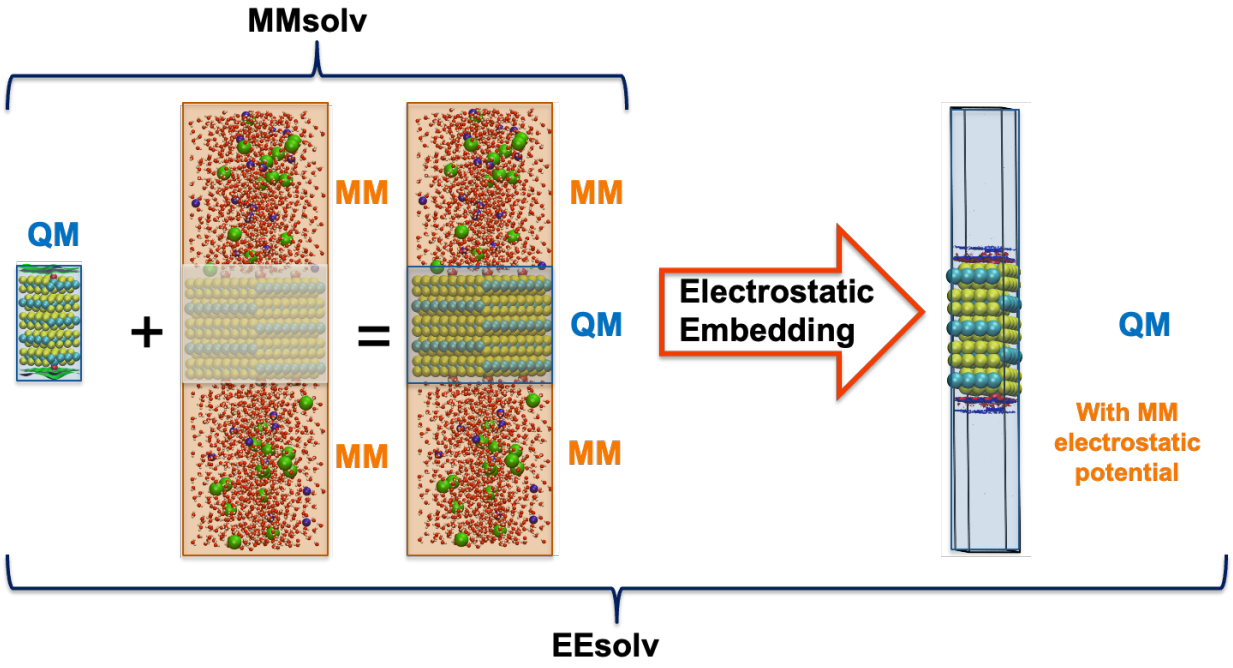

Figure 1: Schematic of our approximate QM/MM schemes. In MMsolv the QM/MM energy is a simple addition of the QM energy plus a MM-derived solvation free energy. With the electrostatic embedding developed herein (EEsolv) the charge distribution of the MM level is utilized to determine a corrected QM energy accounting for the electrostatic interaction between the two subsystems. In principle the scheme can be made self-consistent by cycling between QM and MM, see also Fig. 2.

Under periodic boundary conditions the unit cells have to be neutral. Hence, computing

the electrostatic solvation energy component becomes dependent on the size of the unit cell and various (approximate) corrections are required to remove the spurious contribution of the unavoidable homogeneous background charge.[51] Establishing these corrections consistently for arbitrary QM and the MM subsystems is cumbersome. As an alternative, we here evaluate G_{el} at the QM level through the embedding of the QM subsystem in the charge-distribution of the MM subsystem (see Fig. 1). The G_{non-el} interaction is, however, still determined by FEP or TI, leading to what we call EEsolv:

$$\Delta G_{solv}^{EEsolv} = G_{el}^{QM} + G_{non-el}^{MM} \tag{5}$$

In order to assess the electrostatic interaction energy between the solvent and the solute, the solvent and electrolyte charge distribution as obtained by the sampling at the MM level needs to be included at the DFT level (see Fig. 2 for a schematic). In order to be compatible with the plane-wave DFT description, the MM-derived point-charges are represented as sharp Gaussian charges. We refer the interested reader to section S1 for the details of the freely available implementation in VASPsol and the practical aspects thereof. Here, we just note that the centers of the charges are read by VASPEE in Cartesian coordinates and that no other parameters are required, i.e, VASPEE does neither rely on relative dielectric constants nor on iso-electron density-based cavities. The width of the Gaussians is automatically determined to be 1.6 times the largest FFT grid-spacing (in our case about 0.07 Å), just like for the nuclear charges in VASPsol.[52] This allows a flexible (but minimal) user input, from one to millions of charges.

3 Computational Details

All DFT computations have been performed with VASP,[53,54] linked to a (modified) version of VASPsol to enable the use of point-charges, tentatively called VASPEE. The core-electron interaction are described by the PAW formalism[55,56] using the standard pseudopotentials.

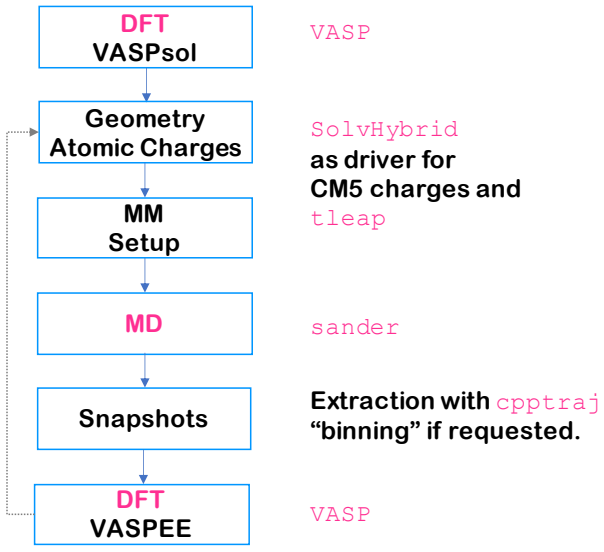

Figure 2: Flow chart for a typical use of VASPEE for an electrified interface. Computationally heavy steps are indicated in pink on the left and the used external codes are mentioned on the right. Since the VASPEE implementation is general, the generation of the point-charge distribution could be performed with any suitable code, i.e., sander is just an example. The grey arrow on the left indicates the self-consistent EEsolv strategy.

The functional was chosen to be the dispersion corrected generalized gradient approximation, PBE-dDsC.[57,58] If not specified otherwise, the plane-wave cutoff was set to 500 eV, and the settings for the numerical grids were "accurate". The wavefunctions have been converged to an energy threshold below 10^{-5} eV. All DFT surfaces are plane symmetric around the central MoS_2 layer.

All molecular dynamics (MD) simulations have been carried out by AMBER[59] and are driven by a modified version of the SolvHybrid package.[40] The geometries of the DFT subsystems are frozen during the MD runs. The water model was chosen to be TIP3P[60] and the parameters for singly-charged ions (Na^+, Cl^-) were chosen accordingly from the amber force field. If not stated otherwise, the interaction between the DFT subsystem and the MM solvent are described by CM5 point-charges[61] combined with Lennard-Jones parameters obtained by the default combination rules as implemented in tleap, where the parameters for the DFT subsystem are taken from UFF,[62] except for MoS_2 for which more accurate parameters are available.[63] Water molecules were kept in their fixed geometry relying on the

SHAKE algorithm.[64,65]

In a typical setup, the geometry is optimized up to forces below 0.05 eV/Å at the DFT level using VASPsol (isodensity (NC_K) of 0.000250 $e^-/Å^{-1}$). Note that this value has been previously chosen as it precludes the presence of implicit solvent between the weakly bound MoS_2 layers.[66] However, this value is only one tenth of the default, indicating that the resulting model will not solvate the system strongly enough. The issue of (system-specific) tuning of this value has been discussed by several groups,[67–70] without coming up with a generally satisfactory solution. The Debye screening length has been set to 3 Å, representative of 1 M ionic strength. The atomic charges are then extracted and the system prepared via SolvHybrid for a MD run in AMBER. We generally used 2×2 supercells compared to the DFT unit cell. This leads to MM cell sizes with diameters > 20Å, also necessary to accommodate twice the cutoff radius (8 Å) plus the boundary layer (2 Å). The system is optimized for 100 steps, heated to 300 K during 200 ps, equilibrated in the NpT ensemble using the Berendsen barostat[71] for 300 ps and then a production run of 6 ns in the NVT ensemble using a Langevin thermostat is performed. For the equilibration and production runs a finer FFT (roughly two points per Å) and a larger real space cutoff (10 Å) has been used to ensure a good description of the charged interface. The charge of the surfaces was neutralized via a $\sim$ 1 M solution of NaCl. Lower electrolyte concentrations are feasible, but require careful convergence tests, as less ions per volume element will lead to more statistical uncertainty and, eventually, larger supercells (and/or out-of-plane sizes) would be required to simulate $\sim$ 0.01 M solutions. Note, that in the limit of no electrolyte (pure water), the unit cells are no longer neutral and unphysical results should be expected. Snapshots are saved every 1 ps to obtain the charge distribution that is used for VASPEE, leading to averages over 6000 snapshots. Figure S5 and S6 provide convergence tests, showing that already 1200 snapshots would be enough to reach converged results. Furthermore, a binning of 0.25 Å leads to an acceptable accuracy, while reducing the number of charges (and thus the associated computational cost) by about 50%. In our case, this binning

is simply achieved by rounding the coordinates and summing the corresponding charges for each rounded point in space. Note, that this is a not a feature of VASPEE, but an intermediate step between the extraction of MD snapshots and writing out the coordinates of the charges for VASPEE, see Fig. 2. Furthermore, the user is free to remove the solvent on one side of the slab. Although we have not actually tested this, one assumes that this would enable the use of more convenient asymmetric slabs instead of the symmetrized ones presented here.

For all our GC-DFT results we have used -4.44 V as the absolute position of SHE with respect to vacuum. Depending on the solvation model, this value can be estimated based on empirical fitting to known potentials of zero charge of metals.[31,72] In the absence of extensive testing (which would require consistent force fields for a large series of systems), we here simply use the experimental estimate. Given that the average electrostatic potential in the bulk solvent region averages to zero, our QM/MM scheme should not suffer from the difficulties of explicit solvent DFT-MD, where the surface potential of water has to be determined.[7]

4 Results and Discussion

4.1 Solvation Energies from Electrostatic Embedding

As a first "real" example for the use of VASPEE we have computed the electrostatic components of the solvation energy of various systems, see Fig. 3. Starting with the water molecule, we observe that the adopted iso-density value for the implicit solvent (chosen to inhibit implicit solvent going between layers of MoS_2[66]) leads to an under-solvation of water -0.11 eV compared to -0.27 eV according to experiment.[61] This is expected, given that the implicit solvent has been "pushed away" from the solute by these settings. Indeed, finding good, system-specific compromises for the location of the solvent cavity has been found challenging.[67–70] Given the electrostatic solvation energy of water of -0.43 eV obtained by

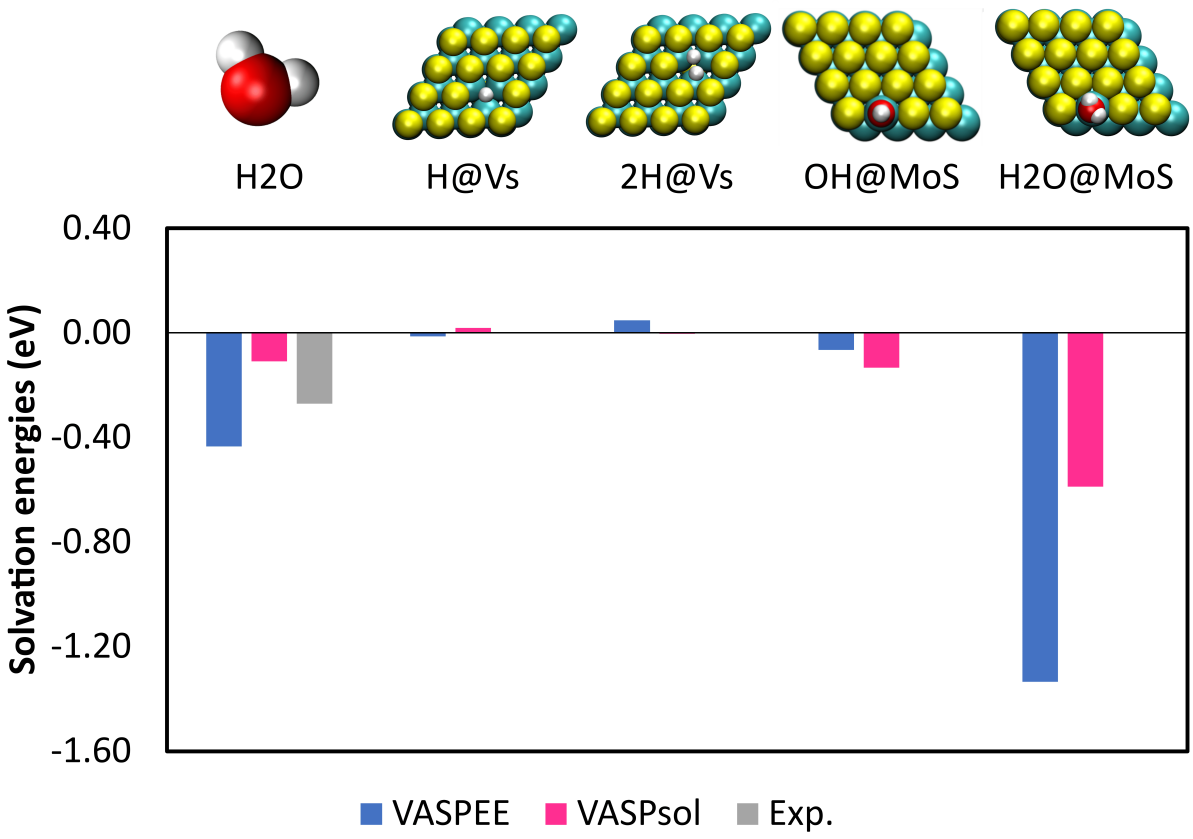

Figure 3: Electrostatic solvation energies obtained with VASPsol and EEsolv for water, two non-polar adsorbates on the sulfur vacancy on the MoS_2 basal plane and two polar adsorbates on the corresponding anti-site defect. The experimental solvation energy of water in water is taken from Ref.[61] and indicated in grey.

VASPEE, we suggest that this approach constitutes a convenient alternative as long as reliable non-bonded interaction parameters between the solvent and the solute are available. For the rather non-polar systems, exemplified by the H-covered sulfur vacancy defects (Vs), the agreement between VASPEE and VASPsol is good, suggesting that in these systems the water solvent does not play a major role. This situation changes, however, for closely related anti-site defects in MoS_2, which we have shown to be covered by OH* or H_2O*.[66] For these quite polar systems the difference between VASPsol and VASPEE are significant, especially for H_2O*. Apparently, the chemisorbed water molecule benefits much more strongly from the solvation at the solid/water interface than the OH* adsorbate.

4.2 Grand-canonical DFT with Electrostatic Embedding

We now turn to the actual target application: The description of charged surfaces. To start with, we analyze the charge distribution of the solvent/electrolyte in the double layer on a positively charged OH* covered anti-site defect of MoS_2 (see Fig. 4). As can be seen from Fig. 4a, the total charge distribution (averages of H_2O and dissolved NaCl) changes significantly when moving from the implicit to the explicit solvent: Not only does an MM-derived charge distribution show more fine-structure, but also the intensity of the polarization is very different. The identification of the origin of this difference in structuring in the double layer is beyond the scope of the present study, but could be due to the competition between the electrostatic and the non-electrostatic interactions. If so, we would expect the difference to be even more pronounced on metallic surfaces, where the near-chemisorption of water leads to a more structured interface.[37] Alternatively, the very high polarization densities of the implicit solvent (blue) might be due to neglected finite-size effects of the structure-less nature implicit solvent, with strong polarizations at the "bare" surface regions for the peak closest to the surface and the second one around the hydrogen atom of OH*. Indeed, a similar structuring (albeit less pronounced and shifted towards larger distances away from the surface) is seen in MM (red). Turning to the charge distribution that is due

to the electrolyte (NaCl), and, thus, makes up the countercharge, Fig. 4b suggests that the countercharge contribution is only responsible for about 1% of the total polarization density. This might explain why previous reports have suggested that achieving realistic counter-charge distributions does not merit significant efforts.[28,73,74] Note that the numerical noise of Fig 4b, itself the result of averaging 6000 snapshots, spaced by 1 ps, i.e., corresponding to a trajectory of 6 ns, has no influence on derived energetics, as already 1200 snapshots provide converged results, see Fig. S6.

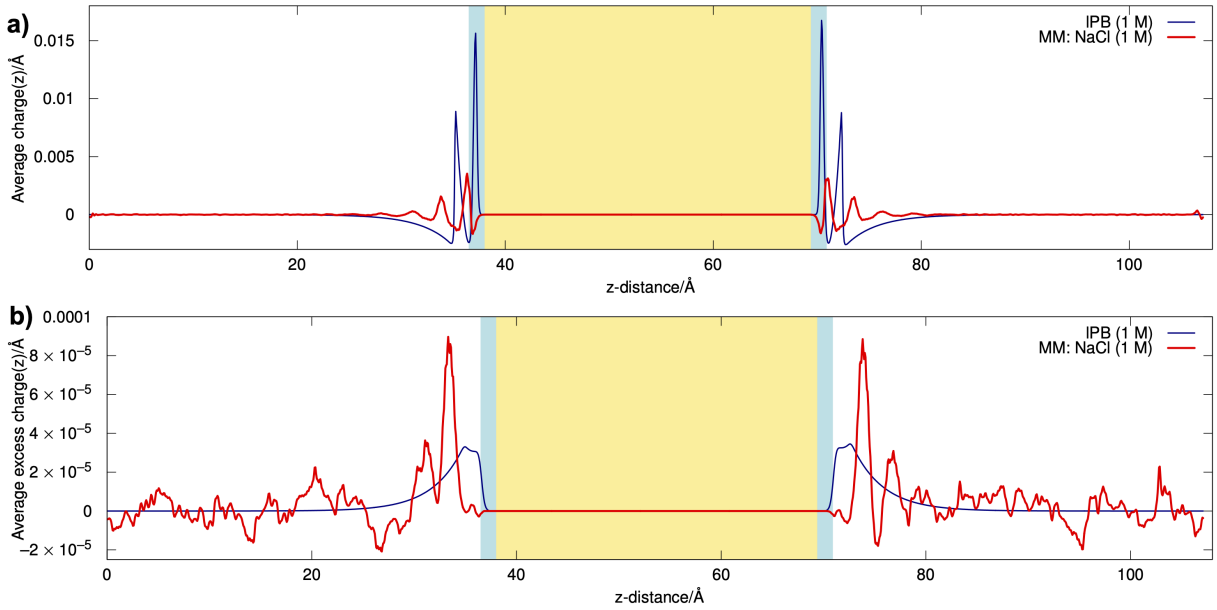

Figure 4: Average charge polarization density across the unit cell for a symmetric OH* covered anti-site defect of MoS_2 for VASPsol (lPB) in blue and EEsolv (NaCl) in red. The top (a) shows the total (solvent plus electrolyte), while the bottom (b) only shows the contribution of the countercharge distribution. The yellow zones correspond to the volume occupied by MoS_2 and the blue zone indicates the location of OH*. The system has a 0.5 positive charge for the VASP unit cell, corresponding to a +2 positive charge for the 2×2 MM unit cell. The electrolyte in the MM unit cell consists of 27 Na^+ and 29 Cl^- ions, dissolved in 1619 water molecules.

Then we analyse the grand-canonical energy as a function of the electrochemical potential. Still using the same model system to exemplify the effect of EEsolv, Figure 5 shows the significantly different behavior when using the implicit and the explicit solvent. The first observation is that EEsolv leads to a reasonably parabolic behavior, with the maximum

being at the potential of zero charge as required for such a capacitor (see also ref[18] and discussion therein). This gives us further confidence that the scheme is working consistently across the range of charges investigated. The second observation is that towards the negative potentials (which are the ones of interest for HER) the curvature (capacitance) is very similar for VASPEE and VASPsol. In other words, the stabilization of the negative surface charge is quite well captured by the linearized Poisson-Boltzmann (lPB) equation, even though the solvent is quite "far away" from the surface. However, the potential of zero charge and the capacitance for the positively charged surface differ: Indeed, the asymmetry between the positive and negative surface-charges is significantly more pronounced at the EEsolv level of theory, presumably because cations (Na^+) and anions (Cl^-) have different sizes and solvation shells.[75]

Now that we have gained confidence in the viability of EEsolv, we turn to the hydrogen evolution reaction. Figure 6 shows the adsorption energy as a function of the electrochemical potential of hydrogen on two potential active sites on the basal-plane of MoS_2:[66] the sulfur vacancy and the OH* covered anti-site defect. One recognizes that for the apolar active site, the two approaches coincide. In other words, the explicit and implicit solvation models solvate these geometries to a similar extent. This is in good agreement with the weak interaction of water molecules with this defect determined at the DFT level,[66] but also with the rather weakly interacting Lennard-Jones potentials.[63] Therefore, the good agreement between EEsolv and the implicit solvent could have been expected.

This situation changes dramatically when moving to OH* on the anti-site defect. As already seen in Fig. 3, the chemisorbed water molecule is significantly more solvated at the interface compared to OH* when using explicit solvation instead of the continuum model. This increases the strength of the adsorption energy of the proton/electron pair on the active site, so that a higher thermodynamic overpotential would be required to drive HER according to EEsolv, compared to the implicit solvent (0.2 V vs 0 V, see Table S3).

According to experiments, the HER reaction over MoS_2 is dominated by active sites on

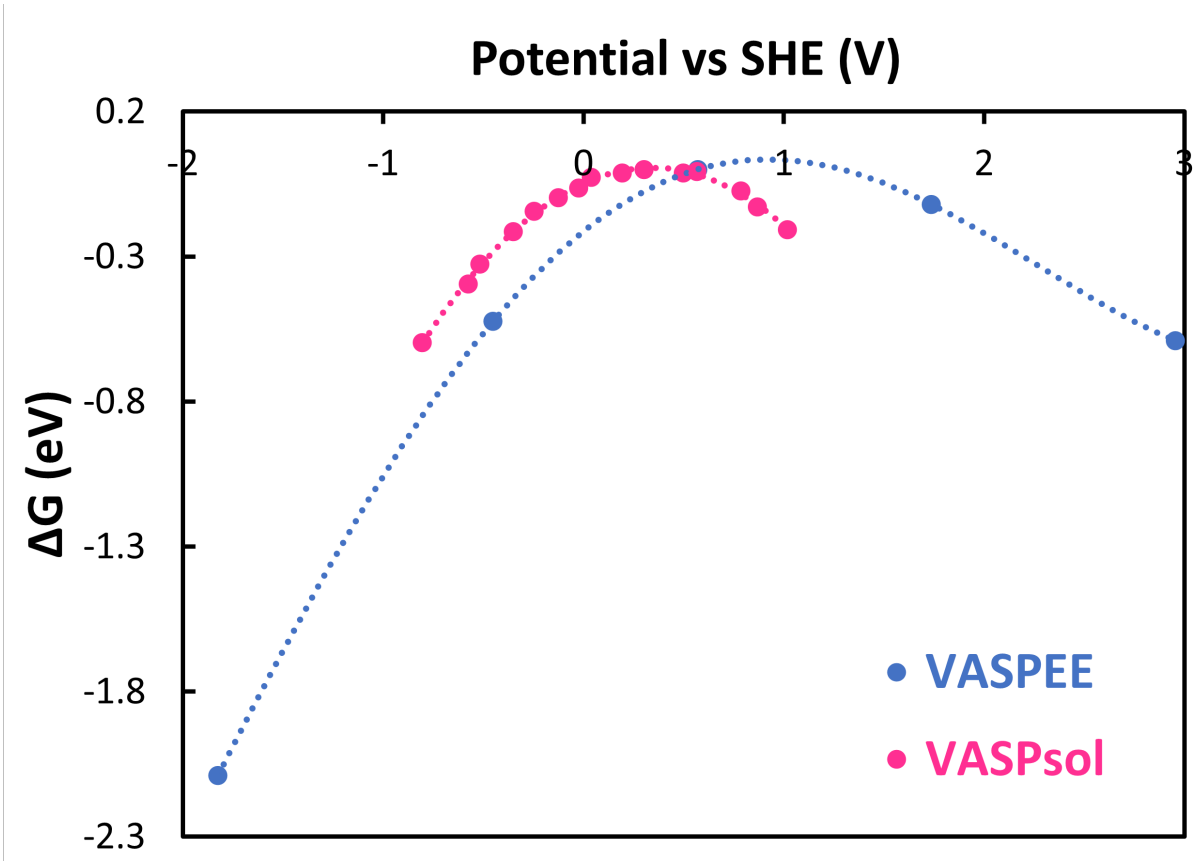

Figure 5: Grand-canonical free energy (see Eq. 2) for OH* adsorbed on the anti-site defect. The 2×2 super-cell compared to DFT has been charged with +1 and +2 electron/Na^+ pairs for the negative potentials and with -1 and -2 electron/Cl^- pairs for the positive potentials. The energy of the neutral, VASPsol-solvated surface is taken as the reference.

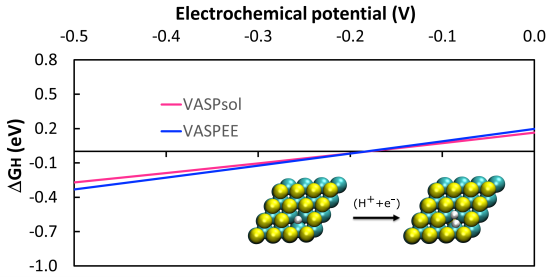

(a) sulfur vacancy

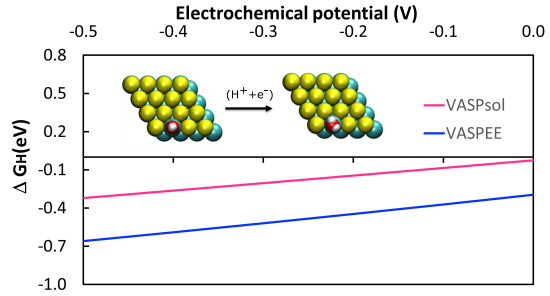

(b) anti-site

Figure 6: Adsorption energy of $H^+ + e^-$ as a function of the electrochemical potential on the sulfur vacancy (a) and the OH* covered anti-site defect (b).

the edges.[76] Previously, we have assessed the activity and stability of these edges sites by GC-DFT in combination with VASPsol.[66,77] Here, we revisit their activity with VASPEE (Figure. 7). The first active site closely resembles the one of Fig. 6b, i.e., it is a chemisorbed OH*. Again, VASPEE solvates H_2O significantly more strongly, suggesting that the Heyrovsky step (liberation of H_2) will be limiting. The thermodynamic overpotential turns out to be equivalent and low (0.1 V), leaving the conclusion of a highly active catalytic site unchanged. In contrast, the hydrogen adsorption on the "second" active site is destabilized in VASPEE compared to the implicit solvent, leading to prohibitively high thermodynamic overpotential of 0.7 V.

Having analysed four possible active sites of MoS_2, we have evidenced non-trivial differences between the implicit and QM/MM description of the solvent effects. In other words, comparing the activity of apolar and polar active sites critically depends on the description of their solvation, suggesting that QM/MM should be routinely replace the less realistic

implicit solvent model.

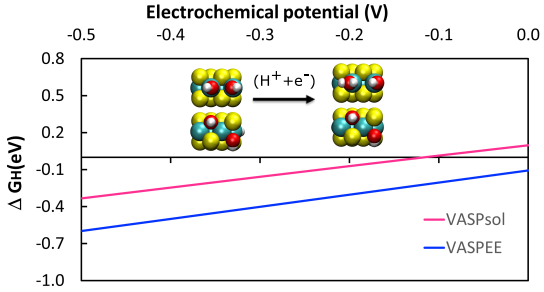

(a) Mo-edge

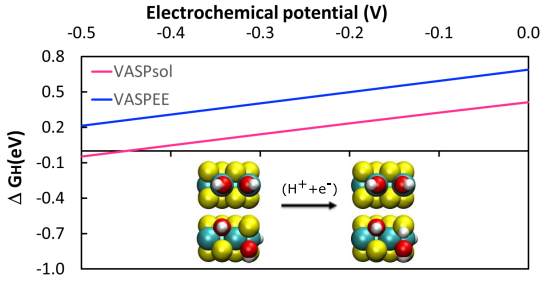

(b) S-edge

Figure 7: Adsorption energy of $H^+ + e^-$ as a function of the electrochemical potential on the Mo-edge covered by OH* (a) and the sulfur atom of S-edge (b).

5 Conclusion

We have implemented an electrostatic embedding for the widely used electronic structure code VASP, calling it VASPEE. The usefulness of the electrostatic embedding in VASP has been illustrated by the computation of hybrid quantum-mechanical/molecular mechanics solvation energies of solid/liquid interfaces, where the accuracy of implicit solvents is questionable. Furthermore, we have demonstrated the robustness of VASPEE and the associated sampling at the molecular mechanics level to obtain a representative solvent/electrolyte distribution at the example of two active sites of MoS_2 for the hydrogen evolution reaction. Indeed, VASPEE in combination with an Amber-based phase-space sampling allows to reach a grand-canonical DFT description of electrified interfaces with a more realistic solid/liquid

interface compared to implicit solvents. For these electrified interfaces the DFT surface bears a net charge, which is exactly cancelled by the distribution of the counter-charges within the MM solvent. Analyzing the polarization density from VASPsol and VASPEE, we highlight that the major difference between the two approaches is less the electrolyte (countercharge) distribution, than the polarization of the solvent. As a consequence, VASPEE represents a cost-effective means to study solvation effects at (charged) interfaces.

Acknowledgement

This work was financially supported by Région Auvergne Rhône-Alpes through the project Pack Ambition Recherche 2018 MoSHi. The authors thank the SYSPROD project and AXELERA Pôle de Compétitivité for financial support (PSMN Data Center).

Supporting Information Available

Additional Figures and Tables containing convergence tests. The source code and two minimal working examples are also provided. The source code and scripts is also available on `https://gitlab.com/lch_interfaces`, where VASPsolEE provides the electrostatic embedding and the legacy branch of SolvHybrid the modified scripts for setting up and running the MM simulations.

References

(1) Gonella, G.; Backus, E. H. G.; Nagata, Y.; Bonthuis, D. J.; Loche, P.; Schlaich, A.; Netz, R. R.; Kühnle, A.; McCrum, I. T.; Koper, M. T. M.; Wolf, M.; Winter, B.; Meijer, G.; Campen, R. K.; Bonn, M. Water at Charged Interfaces. *Nat Rev Chem* **2021**, *5*, 466–485.

(2) Baskin, A.; Prendergast, D. Exploring Chemical Speciation at Electrified Interfaces Using Detailed Continuum Models. *J. Chem. Phys.* **2019**, *150*, 041725.

(3) Huang, J.; Chen, S.; Eikerling, M. Grand-Canonical Model of Electrochemical Double Layers from a Hybrid Density–Potential Functional. *J. Chem. Theory Comput.* **2021**, *17*, 2417–2430.

(4) Favaro, M.; Jeong, B.; Ross, P. N.; Yano, J.; Hussain, Z.; Liu, Z.; Crumlin, E. J. Unravelling the Electrochemical Double Layer by Direct Probing of the Solid/Liquid Interface. *Nat. Commun.* **2016**, *7*, 12695.

(5) Guo, Z.; Ambrosio, F.; Chen, W.; Gono, P.; Pasquarello, A. Alignment of Redox Levels at Semiconductor–Water Interfaces. *Chem. Mater.* **2018**, *30*, 94–111.

(6) Surendralal, S.; Todorova, M.; Neugebauer, J. Impact of Water Coadsorption on the Electrode Potential of H-Pt(1 1 1)-Liquid Water Interfaces. *Phys. Rev. Lett.* **2021**, *126*, 166802.

(7) Santos, E.; Schmickler, W. The Potential of Zero Charge of a Metal Electrode and the Surface Potential of Water from Simulations. *Curr. Opin. Electrochem.* **2023**, *38*, 101208.

(8) Mermin, N. D. Thermal Properties of the Inhomogeneous Electron Gas. *Phys. Rev.* **1965**, *137*, A1441–A1443.

(9) Nalewajski, R. F.; Parr, R. G. Legendre Transforms and Maxwell Relations in Density Functional Theory. *J. Chem. Phys.* **1982**, *77*, 399–407.

(10) Bureau, C.; Lécayon, G. On a Modeling of Voltage-application to Metallic Electrodes Using Density Functional Theory. *J. Chem. Phys.* **1997**, *106*, 8821–8829.

(11) Melander, M. M. Grand Canonical Ensemble Approach to Electrochemical Thermodynamics, Kinetics, and Model Hamiltonians. *Curr. Opin. Electrochem.* **2021**, *29*, 100749.

(12) Abidi, N.; Lim, K. R. G.; Seh, Z. W.; Steinmann, S. N. Atomistic Modeling of Electrocatalysis: Are we There yet? *WIREs Computational Molecular Science* **2021**, *11*, e1499.

(13) Warburton, R. E.; Soudackov, A. V.; Hammes-Schiffer, S. Theoretical Modeling of Electrochemical Proton-Coupled Electron Transfer. *Chem. Rev.* **2022**, *122*, 10599–10650.

(14) Lautar, A. K.; Hagopian, A.; Filhol, J.-S. Modeling interfacial electrochemistry: concepts and tools. *Phys. Chem. Chem. Phys.* **2020**, *22*, 10569–10580.

(15) Letchworth-Weaver, K.; Arias, T. A. Joint density functional theory of the electrode-electrolyte interface: Application to fixed electrode potentials, interfacial capacitances, and potentials of zero charge. *Phys. Rev. B* **2012**, *86*, 075140.

(16) Melander, M. M.; Kuisma, M. J.; Christensen, T. E. K.; Honkala, K. Grand-canonical Approach to Density Functional Theory of Electrocatalytic Systems: Thermodynamics of Solid-liquid Interfaces at Constant Ion and Electrode Potentials. *J. Chem. Phys.* **2018**, *150*, 041706.

(17) Hörmann, N. G.; Andreussi, O.; Marzari, N. Grand Canonical Simulations of Electrochemical Interfaces in Implicit Solvation Models. *J. Chem. Phys.* **2019**, *150*, 041730.

(18) Wei, Z.; Göltl, F.; Steinmann, S. N.; Sautet, P. Modeling Electrochemical Processes with Grand Canonical Treatment of Many-Body Perturbation Theory. *J. Phys. Chem. Lett.* **2022**, *13*, 6079–6084.

(19) Schwarz, K.; Sundararaman, R. The Electrochemical Interface in First-principles Calculations. *Surf. Sci. Rep.* **2020**, *75*, 100492.

(20) Jeanmairet, G.; Levesque, M.; Borgis, D. Tackling Solvent Effects by Coupling Electronic and Molecular Density Functional Theory. *J. Chem. Theory Comput.* **2020**, *16*, 7123–7134.

(21) Haruyama, J.; Ikeshoji, T.; Otani, M. Electrode Potential from Density Functional Theory Calculations Combined with Implicit Solvation Theory. *Phys. Rev. Materials* **2018**, *2*, 095801.

(22) Taylor, C. D.; Wasileski, S. A.; Filhol, J.-S.; Neurock, M. First Principles Reaction Modeling of the Electrochemical Interface: Consideration and Calculation of a Tunable Surface Potential from Atomic and Electronic structure. *Phys. Rev. B* **2006**, *73*, 165402.

(23) Bonnet, N.; Morishita, T.; Sugino, O.; Otani, M. First-Principles Molecular Dynamics at a Constant Electrode Potential. *Phys. Rev. Lett.* **2012**, *109*, 266101.

(24) Melander, M.; Wu, T.; Honkala, K. Constant Inner Potential DFT for Modelling Electrochemical Systems under Constant Potential and Bias. 2023; `https://chemrxiv.org/engage/chemrxiv/article-details/63fe1546937392db3d34fa4a`.

(25) Kopač Lautar, A.; Bitenc, J.; Rejec, T.; Dominko, R.; Filhol, J.-S.; Doublet, M.-L. Electrolyte Reactivity in the Double Layer in Mg Batteries: An Interface Potential-Dependent DFT Study. *J. Am. Chem. Soc.* **2020**, *142*, 5146–5153.

(26) Jinnouchi, R.; Anderson, A. B. Electronic structure calculations of liquid-solid interfaces: Combination of density functional theory and modified Poisson-Boltzmann theory. *Phys. Rev. B* **2008**, *77*, 245417.

(27) Wang, H.-F.; Liu, Z.-P. Formic Acid Oxidation at Pt/H2O Interface from Periodic DFT Calculations Integrated with a Continuum Solvation Model. *J. Phys. Chem. C* **2009**, *113*, 17502.

(28) Gauthier, J. A.; Dickens, C. F.; Heenen, H. H.; Vijay, S.; Ringe, S.; Chan, K. Unified Approach to Implicit and Explicit Solvent Simulations of Electrochemical Reaction Energetics. *J. Chem. Theory Comput.* **2019**, *15*, 6895–6906.

(29) Fernandez-Alvarez, V. M.; Eikerling, M. H. Interface Properties of the Partially Oxidized Pt(111) Surface Using Hybrid DFT–Solvation Models. *ACS Appl. Mater. Interfaces* **2019**, *11*, 43774–43780.

(30) Truscott, M.; Andreussi, O. Field-Aware Interfaces in Continuum Solvation. *J. Phys. Chem. B* **2019**, *123*, 3513–3524.

(31) Mathew, K.; Kolluru, V. S. C.; Mula, S.; Steinmann, S. N.; Hennig, R. G. Implicit Self-consistent Electrolyte Model in Plane-wave Density-functional Theory. *J. Chem. Phys.* **2019**, *151*, 234101.

(32) Ringe, S.; Hörmann, N. G.; Oberhofer, H.; Reuter, K. Implicit Solvation Methods for Catalysis at Electrified Interfaces. *Chem. Rev.* **2022**, *122*, 10777–10820.

(33) Bramley, G. A.; Nguyen, M.-T.; Glezakou, V.-A.; Rousseau, R.; Skylaris, C.-K. Understanding Adsorption of Organics on Pt(111) in the Aqueous Phase: Insights from DFT Based Implicit Solvent and Statistical Thermodynamics Models. *J. Chem. Theory Comput.* **2022**, *18*, 1849–1861.

(34) Saleheen, M.; Heyden, A. Liquid-Phase Modeling in Heterogeneous Catalysis. *ACS Catal.* **2018**, *8*, 2188–2194.

(35) Zhang, X.; DeFever, R. S.; Sarupria, S.; Getman, R. B. Free Energies of Catalytic Species Adsorbed to Pt(111) Surfaces under Liquid Solvent Calculated Using Classical and Quantum Approaches. *J. Chem. Inf. Model.* **2019**, *59*, 2190–2198.

(36) Steinmann, S. N.; Michel, C. How to Gain Atomistic Insights on Reactions at the Water/Solid Interface? *ACS Catal.* **2022**, *12*, 6294–6301.

(37) Steinmann, S. N.; Ferreira De Morais, R.; Götz, A. W.; Fleurat-Lessard, P.; Iannuzzi, M.; Sautet, P.; Michel, C. Force Field for Water over Pt(111): Development, Assessment, and Comparison. *J. Chem. Theory Comput.* **2018**, *14*, 3238–3251.

(38) Rey, J.; Blanck, S.; Clabaut, P.; Loehlé, S.; Steinmann, S. N.; Michel, C. Transferable Gaussian Attractive Potentials for Organic/Oxide Interfaces. *J. Phys. Chem. B* **2021**, *125*, 10843–10853.

(39) Clabaut, P.; Fleurat-Lessard, P.; Michel, C.; Steinmann, S. N. Ten Facets, One Force Field: The GAL19 Force Field for Water-Noble Metal Interfaces. *J. Chem. Theory Comput.* **2020**, *16*, 4565–4578.

(40) Clabaut, P.; Schweitzer, B.; Goetz, A. W.; Michel, C.; Steinmann, S. N. Solvation Free Energies and Adsorption Energies at the Metal/Water Interface from Hybrid Quantum-Mechanical/Molecular Mechanics Simulations. *J. Chem. Theory Comput.* **2020**, *16*, 6539 – 6549.

(41) Rey, J.; Clabaut, P.; Réocreux, R.; Steinmann, S. N.; Michel, C. Mechanistic Investigation and Free Energies of the Reactive Adsorption of Ethanol at the Alumina/Water Interface. *J. Phys. Chem. C* **2022**, *126*, 7446–7455.

(42) Garza, A. J. Solvation Entropy Made Simple. *J. Chem. Theory Comput.* **2019**, *15*, 3204–3214.

(43) Fdez Galvan, I.; Sanchez, M.; Martin, M.; Olivares del Valle, F.; Aguilar, M. ASEP/MD: A Program for the Calculation of Solvent Effects Combining QM/MM Methods and the Mean Field Approximation. *Comp. Phys. Commun.* **2003**, *155*, 244–259.

(44) Lim, H.-K.; Lee, H.; Kim, H. A Seamless Grid-Based Interface for Mean-Field QM/MM Coupled with Efficient Solvation Free Energy Calculations. *Journal of Chemical Theory and Computation* **2016**, *12*, 5088–5099.

(45) González-Espinoza, C. E.; Rumble, C. A.; Borgis, D.; Wesolowski, T. A. Quantifying Fluctuations of Average Solvent Environments for Embedding Calculations. *J. Chem. Theory Comput.* **2022**, *18*, 1072–1088.

(46) Elliott, J. D.; Troisi, A.; Carbone, P. A QM/MD Coupling Method to Model the Ion-Induced Polarization of Graphene. *J. Chem. Theory Comput.* **2020**, *16*, 5253–5263.

(47) Shin, S.-J.; Kim, D. H.; Bae, G.; Ringe, S.; Choi, H.; Lim, H.-K.; Choi, C. H.; Kim, H. On the Importance of the Electric Double Layer Structure in Aqueous Electrocatalysis. *Nat Commun* **2022**, *13*, 174.

(48) Dohn, A. O.; Jónsson, E. Ö.; Levi, G.; Mortensen, J. J.; Lopez-Acevedo, O.; Thygesen, K. S.; Jacobsen, K. W.; Ulstrup, J.; Henriksen, N. E.; Møller, K. B.; Jónsson, H. Grid-Based Projector Augmented Wave (GPAW) Implementation of Quantum Mechanics/Molecular Mechanics (QM/MM) Electrostatic Embedding and Application to a Solvated Diplatinum Complex. *J. Chem. Theory Comput.* **2017**, *13*, 6010–6022.

(49) Giannozzi, P.; Andreussi, O.; Brumme, T.; Bunau, O.; Nardelli, M. B.; Calandra, M.; Car, R.; Cavazzoni, C.; Ceresoli, D.; Cococcioni, M.; Colonna, N.; Carnimeo, I.; Corso, A. D.; Gironcoli, S. d.; Delugas, P.; DiStasio, R. A.; Ferretti, A.; Floris, A.; Fratesi, G.; Fugallo, G.; Gebauer, R.; Gerstmann, U.; Giustino, F.; Gorni, T.; Jia, J.; Kawamura, M.; Ko, H.-Y.; Kokalj, A.; Küçükbenli, E.; Lazzeri, M.; Marsili, M.; Marzari, N.; Mauri, F.; Nguyen, N. L.; Nguyen, H.-V.; Otero-de-la Roza, A.; Paulatto, L.; Poncé, S.; Rocca, D.; Sabatini, R.; Santra, B.; Schlipf, M.; Seitsonen, A. P.; Smogunov, A.; Timrov, I.; Thonhauser, T.; Umari, P.; Vast, N.; Wu, X.; Baroni, S. Advanced Capabilities for Materials Modelling with Quantum ESPRESSO. *J. Phys.: Condens. Matter* **2017**, *29*, 465901.

(50) Steinmann, S. N.; Sautet, P.; Michel, C. Solvation Free Energies for Periodic Surfaces: Comparison of Implicit and Explicit Solvation Models. *Phys. Chem. Chem. Phys.* **2016**, *18*, 31850–31861.

(51) Blumberger, J.; Bernasconi, L.; Tavernelli, I.; Vuilleumier, R.; Sprik, M. Electronic

Structure and Solvation of Copper and Silver Ions: A Theoretical Picture of a Model Aqueous Redox Reaction. *J. Am. Chem. Soc.* **2004**, *126*, 3928–3938.

(52) Mathew, K.; Sundararaman, R.; Letchworth-Weaver, K.; Arias, T. A.; Hennig, R. G. Implicit Solvation Model for Density-functional Study of Nanocrystal Surfaces and Reaction Pathways. *J. Chem. Phys.* **2014**, *140*, 084106.

(53) Kresse, G. Ab Initio Molecular Dynamics for Liquid Metals. *Journal of Non-Crystalline Solids* **1995**, *192-193*, 222–229.

(54) Kresse, G.; Furthmüller, J. Efficient Iterative Schemes for *ab initio* Total-energy Calculations Using a Plane-wave Basis Set. *Physical Review B* **1996**, *54*, 11169–11186.

(55) Blochl, P. E. Projector Augmented-wave Method. *Phys. Rev. B* **1994**, *50*, 17953.

(56) Kresse, G.; Joubert, D. From Ultrasoft Pseudopotentials to the Projector Augmented-wave Method. *Phys. Rev. B* **1999**, *59*, 1758–1775.

(57) Perdew, J. P.; Burke, K.; Ernzerhof, M. Generalized Gradient Approximation Made Simple. *Phys. Rev. Lett.* **1996**, *77*, 3865–3868.

(58) Steinmann, S. N.; Corminboeuf, C. Comprehensive Benchmarking of a Density-Dependent Dispersion Correction. *J. Chem. Theory Comput.* **2011**, *7*, 3567–3577.

(59) Case, D. A.; Cheatham, T. E.; Darden, T.; Gohlke, H.; Luo, R.; Merz, K. M.; Onufriev, A.; Simmerling, C.; Wang, B.; Woods, R. J. The Amber Biomolecular Simulation Programs. *J. Comput. Chem.* **2005**, *26*, 1668–1688.

(60) Jorgensen, W. L.; Chandrasekhar, J.; Madura, J. D.; Impey, R. W.; Klein, M. L. Comparison of Simple Potential Functions for Simulating Liquid Water. *J. Chem. Phys.* **1983**, *79*, 926–935.

(61) Marenich, A. V.; Jerome, S. V.; Cramer, C. J.; Truhlar, D. G. Charge Model 5: An Extension of Hirshfeld Population Analysis for the Accurate Description of Molecular

Interactions in Gaseous and Condensed Phases. *J. Chem. Theory Comput.* **2012**, *8*, 527–541.

(62) Rappe, A. K.; Casewit, C. J.; Colwell, K. S.; Goddard, W. A.; Skiff, W. M. UFF, a Full Periodic Table Force Field for Molecular Mechanics and Molecular Dynamics Simulations. *J. Am. Chem. Soc.* **1992**, *114*, 10024–10035.

(63) Sresht, V.; Govind Rajan, A.; Bordes, E.; Strano, M. S.; Padua, A. A.; Blankschtein, D. Quantitative Modeling of MoS2–Solvent Interfaces: Predicting Contact Angles and Exfoliation Performance Using Molecular Dynamics. *J. Phys. Chem. C* **2017**, *121*, 9022–9031.

(64) Ryckaert, J.-P.; Ciccotti, G.; Berendsen, H. J. Numerical Integration of the Cartesian Equations of Motion of a System With Constraints: Molecular Dynamics of n-Alkanes. *J. Comput. Phys.* **1977**, *23*, 327–341.

(65) Ryckaert, J. Special Geometrical Constraints in the Molecular Dynamics of Chain Molecules. *Mol. Phys.* **1985**, *55*, 549–556.

(66) Abidi, N.; Bonduelle-Skrzypczak, A.; Steinmann, S. N. Revisiting the Active Sites at the MoS2/H2O Interface via Grand-Canonical DFT: The Role of Water Dissociation. *ACS applied materials & interfaces* **2020**, *12*, 31401–31410.

(67) Lespes, N.; Filhol, J.-S. Using Implicit Solvent in Ab Initio Electrochemical Modeling: Investigating Li+/Li Electrochemistry at a Li/Solvent Interface. *J. Chem. Theory Comput.* **2015**, *11*, 3375–3382.

(68) Gauthier, J. A.; Ringe, S.; Dickens, C. F.; Garza, A. J.; Bell, A. T.; Head-Gordon, M.; Nørskov, J. K.; Chan, K. Challenges in Modeling Electrochemical Reaction Energetics with Polarizable Continuum Models. *ACS Catal.* **2019**, *9*, 920–931.

(69) Bramley, G.; Nguyen, M.-T.; Glezakou, V.-A.; Rousseau, R.; Skylaris, C.-K. Reconciling Work Functions and Adsorption Enthalpies for Implicit Solvent Models: A Pt (111)/Water Interface Case Study. *J. Chem. Theory Comput.* **2020**, *16*, 2703–2715.

(70) Aziz, A.; Carrasco, J. Modeling Magnesium Surfaces and their Dissolution in an Aqueous Environment Using an Implicit Solvent Model. *J. Chem. Phys.* **2022**, *156*, 174702.

(71) Berendsen, H. J. C.; Postma, J. P. M.; van Gunsteren, W. F.; DiNola, A.; Haak, J. R. Molecular Dynamics with Coupling to an External Bath. *The Journal of Chemical Physics* **1984**, *81*, 3684–3690.

(72) Sundararaman, R.; Goddard, W. A. The Charge-asymmetric Nonlocally Determined Local-electric (CANDLE) Solvation Model. *J. Chem. Phys.* **2015**, *142*, 064107.

(73) Kastlunger, G.; Lindgren, P.; Peterson, A. A. Controlled-Potential Simulation of Elementary Electrochemical Reactions: Proton Discharge on Metal Surfaces. *J. Phys. Chem. C* **2018**, *122*, 12771–12781.

(74) Hagopian, A.; Doublet, M.-L.; Filhol, J.-S.; Binninger, T. Advancement of the Homogeneous Background Method for the Computational Simulation of Electrochemical Interfaces. *J. Chem. Theory Comput.* **2022**, *18*, 1883–1893.

(75) Staub, R.; Steinmann, S. N. Parameter-free Coordination Numbers for Solutions and Interfaces. *J. Chem. Phys.* **2020**, *152*, 024124.

(76) Jaramillo, T. F.; Jørgensen, K. P.; Bonde, J.; Nielsen, J. H.; Horch, S.; Chorkendorff, I. Identification of Active Edge Sites for Electrochemical H2 Evolution from MoS2 Nanocatalysts. *science* **2007**, *317*, 100–102.

(77) Abidi, N.; Bonduelle-Skrzypczak, A.; Steinmann, S. N. How Stable Are 2H-MoS2 Edges under Hydrogen Evolution Reaction Conditions? *J. Phys. Chem. C* **2021**, *125*, 17058–17067.

Graphical TOC Entry